Old Dominion University
ODU Digital Commons

Bioelectrics Publications

Frank Reidy Research Center for Bioelectrics

2015

Picosecond to Terahertz Perturbation of Interfacial Water and Electropermeabilization of Biological Membranes

P. Thomas Vernier
Old Dominion University

Zachary A. Levine

Ming-Chak Ho

Shu Xiao
Old Dominion University

Iurii Semenov
Old Dominion University

See next page for additional authors

Follow this and additional works at: https://digitalcommons.odu.edu/bioelectrics_pubs

Part of the Biochemistry Commons, Cell Biology Commons, and the Physiology Commons

Authors

P. Thomas Vernier, Zachary A. Levine, Ming-Chak Ho, Shu Xiao, Iurii Semenov, and Andrei G. Pakhomov

Picosecond and Terahertz Perturbation of Interfacial Water and Electropermeabilization of Biological Membranes

P. Thomas Vernier[1], **Zachary A. Levine**[2,3], **Ming-Chak Ho**[4], **Shu Xiao**[1], **Iurii Semenov**[1], and **Andrei G. Pakhomov**[1]

[1]Frank Reidy Research Center for Bioelectrics, Old Dominion University, Norfolk, VA, USA

[2]Department of Physics, University of California Santa Barbara, Santa Barbara, CA, USA

[3]Department of Chemistry and Biochemistry, University of California Santa Barbara, Santa Barbara, CA, USA

[4]Department of Physics and Astronomy, University of Southern California, Los Angeles, CA, USA

Abstract

Nonthermal probing and stimulation with subnanosecond electric pulses and terahertz electromagnetic radiation may lead to new, minimally invasive diagnostic and therapeutic procedures and to methods for remote monitoring and analysis of biological systems, including plants, animals, and humans. To effectively engineer these still-emerging tools, we need an understanding of the biophysical mechanisms underlying the responses that have been reported to these novel stimuli. We show here that subnanosecond (500 ps) electric pulses induce action potentials in neurons and cause calcium transients in neuroblastoma-glioma hybrid cells, and we report complementary molecular dynamics simulations of phospholipid bilayers in electric fields in which membrane permeabilization occurs in less than 1 ns. Water dipoles in the interior of these model membranes respond in less than 1 ps to permeabilizing electric potentials by aligning in the direction of the field, and they re-orient at terahertz frequencies to field reversals. The mechanism for subnanosecond lipid electropore formation is similar to that observed on longer time scales — energy-minimizing intrusions of interfacial water into the membrane interior and subsequent reorganization of the bilayer into hydrophilic, conductive structures.

Keywords

Introduction

In recent years, investigations of the effects of ultra-short electric pulses on biological systems have probed shorter and shorter time scales, reaching now even into the picosecond range (Schoenbach et al. 2008; Xiao et al. 2011; Camp et al. 2012). Because picosecond

Corresponding author: P. Thomas Vernier, Frank Reidy Research Center for Bioelectrics, Old Dominion University, 4211 Monarch Way, Norfolk, VA, 23508, USA, pvernier@odu.edu +1 757 683 7046.

electric pulses have very fast rise times, they contain significant amounts of energy in the gigahertz and terahertz spectral regions, and we note that on this separate track studies of biological responses to terahertz electromagnetic radiation (with picosecond polarity reversals) have also expanded over the past few years, as terahertz sources have become more accessible. Some investigators report no effects of terahertz exposures (Zeni et al. 2007; Williams et al. 2011; Hintzsche et al. 2013). Where responses are observed (Ramundo-Orlando and Gallerano 2009), some appear to be associated with temperature increases (Wilmink et al. 2011), but others seem to be caused by direct, temperature-independent interactions of electric fields with biological processes (Titova et al. 2013a; Titova et al. 2013b). Millimeter waves, an electromagnetic regime that may be considered to overlap with terahertz radiation, have also been reported to affect biological systems (Ramundo-Orlando et al. 2007; Kim et al. 2013; Albini et al. 2014; Romanenko et al. 2014), and these phenomena may be related. Because effects from both picosecond pulses and terahertz radiation imply electric-field-driven biomolecular rearrangements on the picosecond time scale, the mechanisms for the two sets of phenomena are likely to be related, and it may be beneficial to consider them together.

Apart from the functional stimulation of electrically active cells, the most reproducible, least ambiguous, and best understood non-thermal bio-effect of pulsed electric fields is the permeabilization of membranes, a process called electroporation or electropermeabilization (Teissié and Rols 1993; Rols 2006.). In the presence of an external electric field of sufficient magnitude and duration, permeabilizing structures form in cell membranes, breaching the normal barrier function and permitting the transport of normally impermeant materials into or out of the cell (Neumann et al. 1982; Marty et al. 2006; Heller and Heller 2006; Frandsen et al 2012).

Most electroporation protocols for laboratory, clinical, and biotechnological applications use pulses with durations of at least 100 μs, but membrane permeabilization occurs with pulses shorter than 100 ns (Pakhomov et al. 2007a) or even 10 ns (Benz and Zimmermann 1980; Vernier et al 2006a). Permeabilization of cell membranes with submicrosecond pulsed electric fields is accompanied by a host of other effects, many of which are consequences of the initial breaching of membrane integrity observed not only for the plasma membrane but also for intracellular, membrane-bound structures (Schoenbach et al. 2001; Vernier et al. 2003; Vernier et al. 2004; Tekle et al. 2005; Nuccitelli et al. 2006; Pakhomov et al. 2007b; Craviso et al. 2010; Napotnik et al. 2010; Ibey et al. 2011; Batista Napotnik et al. 2012; Pakhomova et al. 2012; Silve et al. 2012; Tolstykh et al. 2014).

"Long-pulse" (> 100 ns) electroporation models treat the membrane as a capacitor which is charged by ions migrating in the applied electric field until a critical transmembrane potential is reached and permeabilizing structures are formed (Coster 1965; Zimmermann et al. 1974; Abidor et al. 1979; Sugar and Neumann 1984; Weaver and Chizmadzhev 1996; Neu and Krassowska 1999). As the pulse duration (the time during which the membrane is charged) is reduced, higher and higher fields are needed for detectable permeabilization (Vernier et al. 2006a; Ibey et al. 2010). For very short pulses (< 10 ns), however, if the field is high enough (> 1 MV/m), a porating field develops across the membrane from dielectric effects alone, and the contribution of charge migration to the permeabilization process

becomes less significant (Kotnik and Miklavcic 2000; Gowrishankar and Weaver 2003; Timoshkin et al. 2006).

In one report, *subnanosecond* pulses of 800 ps duration produced membrane permeabilization at physiological temperatures only after exposures that involved either very large numbers (hundreds) of pulses or very high external fields (>10 MV/m) (Schoenbach et al. 2008). Permeabilization with 200 ps pulses requires even stronger doses — thousands of pulses when the field is 25 MV/m (Xiao et al. 2011). Interestingly, fields greater than 10 MV/m are reported to produce non-thermal effects from exposures of cells to terahertz electromagnetic fields (EMF) (Wilmink et al. 2011; (Titova et al. 2013b)

The mechanism for the permeabilizing restructuring of the membrane that occurs in all of these regimes remains an open question (Teissié et al. 2005). Molecular dynamics simulations provide a view of one type of permeabilizing structure, the lipid electropore (Tieleman 2004; Gurtovenko and Vattulainen 2005; Tarek 2005; Böckmann et al. 2008; Levine and Vernier 2010), consistent with experimental observations (Melikov et al. 2001; Naumowicz and Figaszewski 2013; Koronkiwicz et al. 2002) and continuum models (Zimmermann et al. 1974; Abidor et al. 1979; Chizmadzhev and Abidor 1980; Weaver and Chizmadzhev 1996). The formation of these nanometer-scale, conductive pores is initiated by the electric-field-stabilized intrusion of interfacial water into the membrane interior, which leads to the construction of energy-minimized water bridges across the lipid bilayer and the reorganization of the membrane phospholipids along the water columns to form the hydrophilic wall of the pore (Tokman et al. 2013). Although lipid electropores are only one component of the electropermeabilized cell membrane, they are the first structures to form after the application of a porating electric field, and it may be that for very short pulses or very high-frequency EMF they are the dominant structures.

Lipid electropore formation is a stochastic process, with the probability of a pore forming at a given location increasing as an exponential function of the transmembrane electric field (Sugar and Neumann 1984; Vernier et al. 2013). This means that fewer pores form at lower fields, at lower areal densities. Once the process is initiated at a given locus, however, construction of a hydrophilic, conductive pore is complete within a nanosecond — less than a nanosecond at higher fields (Levine and Vernier 2010). Continuum and molecular models then, are consistent with the formation of electropores on the picosecond time scale.

Experimental studies of biological systems exposed to electric fields at gigahertz and terahertz frequencies or picosecond pulse durations are challenging from an engineering point of view (parasitic impedances which can be neglected for slower signals must be taken into account), but are essential for validating the models. Here we report recent experimental results and new molecular simulation results that together shed new light on the biophysical initiating steps that lead to such profound disruptions "downstream" — osmotic stress, redistribution of membrane phospholipids, and cell death by apoptosis or other pathways.

Methods

Cell culture

NG108 rat neuroblastoma-glioma hybrid cells (ATCC HB-12317) cells were cultured at 37 °C with 5% CO_2 in air in Dulbecco's Modified Eagle's medium (Caisson Labs, North Logan, UT) without sodium pyruvate, supplemented with 4 mM L-glutamine, 4.5 g/L glucose, 10% FBS, 0.2 mM hypoxanthine, 400 nM aminopterin, and 0.016 mM thymidine (without antibiotics). Media supplements were from Sigma-Aldrich (St. Louis, MO) except for the FBS (Atlanta Biologicals, Norcross, GA). For the passage immediately preceding experiments, cells were transferred onto glass coverslips. Primary rat hippocampus neurons were obtained from Life Technologies (Carlsbad, CA) and seeded on poly-D-lysine/laminin coated coverslips (BD Bioscience, Bedford, MA). The neurons were grown at 37 °C with 5% CO_2 in air in the supplier-recommended medium (Neurobasal medium supplemented with 200 mM GlutaMAX I and 2% of B27, all from Life Technologies).

Calcium imaging

Procedures for loading cells with Fura-2, calibration of the dye, and time-lapse fluorescence imaging were reported previously (Semenov et al. 2013). Briefly, to load the dye, cells on coverslips were incubated for 30 min in physiological buffer (in mM: 140 NaCl, 5.4 KCl, 1.5 $MgCl_2$, 2 $CaCl_2$, 10 glucose, and 10 HEPES, pH 7.2, ~300 mOsm/kg) containing 5 μM Fura-2/AM and 0.02% Pluronic F-127 (Life Technologies, Grand Island, NY), in the dark at room temperature. Then the coverslips were rinsed in buffer without dye and detergent for 15 min and transferred to a glass-bottomed perfusion chamber (Warner Instruments, Hamden, CT) mounted on an Olympus IX71 inverted microscope (Olympus America, Center Valley, PA).

Dual excitation at 340 nm and 380 nm for ratiometric imaging was carried out with a Lambda DG4 wavelength switching system (Sutter Instruments, Novato, CA), with emission measured at 510 nm every 150 ms (20 ms exposure at each wavelength) using a C9100-02 EM CCD camera (Hamamatsu Photonics, Japan). The cytosolic free calcium concentration ($[Ca^{2+}]_i$) was calculated from the Fura-2 emission ratio with a help of Metafluor v.7.5 software (Molecular Devices, Sunnyvale, CA). $[Ca^{2+}]_i$ measurements typically began one minute prior to electric pulse application. In most experiments, fluorescence intensity traces were smoothed with an Origin 8.0 FFT filter utility (OriginLab Corporation Northampton, MA).

Pulse generator and delivery system

Generation of picosecond pulses with an FPG 20-1 pulse generator (FID GmbH, Burbach, Germany) and delivery of the pulses to cells on the stage of an epifluorescence microscope were carried out using methods similar to those previously described (Xiao et al. 2011). For the hippocampal neuron experiments a micro-coaxial cable (outer diameter 310 μm, inner diameter 80 μm) with insulation removed from the last 350 μm to expose the inner conductor, was used to deliver pulses to the cells. The end of the cable was positioned over the cells with a micromanipulator (Fig. 1). The electric field distribution was simulated by a 3-D electric field solver, Amaze (Field Precision, Albuquerque, NM) (Fig. 1). To avoid

blockage of the image by the coaxial cable tip, we chose the two regions near the tip, indicated by the circles. The electric field for these two regions is about 5 MV/m. For this micro-coaxial electrode configuration, the pulse width was about 320 ps (full-width, half-maximum).

For experiments with NG108 neuroblastoma-glioma hybrid cells, pulses were delivered to cells in the bath by means of a pair of tungsten rods (100 μm diameter, 170 μm gap, 3.5 mm long) at the end of a 50 Ω RG316 coaxial cable. The connection is secured with epoxy, which also prevents air breakdown between the rods. Arcing does not occur when the rods are submerged into the aqueous medium covering the cells. The electrode assembly was positioned with an MPC-200 robotic manipulator (Sutter Instruments, Novato, CA), that placed the tips of the rods at precisely 50 μm above the coverslip surface with selected cells being in the middle of the gap between the tips. For this parallel rod electrode configuration, some pulse broadening was observed in simulations, to about 500 ps, but the electric field was 19 MV/m, higher than that in the coaxial electrode configuration.

Pulses were triggered externally and synchronized with image acquisitions by a TTL pulse protocol using a Digidata 1440A board and Clampex v. 10.2 software (Molecular Devices). Timing of pulse delivery, pulse repetition interval, and the number of pulses were all programmed in Clampex. A typical pulse waveform is shown in Fig. 2.

Patch clamp

Whole-cell measurements of plasma membrane potential were performed in current-clamp mode using a Multiclamp 700B amplifier, Digidata 1322A A-D converter, and pCLAMP software (Molecular Devices). For imaging, a coverslip with attached cells was placed into a glass-bottomed chamber on an Olympus IX81/FV1000 confocal laser scanning system. Bath and pipette buffers contained, respectively (in mM): 136 NaCl, 5 KCl, 2 $MgCl_2$, 2 $CaCl_2$, 10 HEPES, 10 glucose (pH 7.4), and: 150 K gluconate, 10 NaCl, 5 K-EGTA, 1 $MgCl_2$, 1 $CaCl_2$, 10 HEPES (pH 7.2).

Molecular dynamics simulations

Simulations were performed using GROMACS version 4.0.5 (Hess et al. 2008) on the University of Southern California High Performance Computing and Communications (HPCC) Linux cluster (http://www.usc.edu/hpcc/). Lipid topologies, water model, thermostat, barostat, bond constraints, equilibration protocols, calculation of electrostatic interactions, and other parameters and procedures were as previously described (Ho et al. 2013). Simulations were run at 310 K in the NPT ensemble. Lipid bilayers are composed of 128 POPC lipids (64 per leaflet) and at least 35 waters/lipid (some systems had 70 waters/lipid; this had no effect on the outcome), with initial system dimensions of approximately 7 nm × 7 nm × 7 nm (10 nm for the systems containing more water). The planes of the water-lipid interface are normal to the z-direction of the simulation box. The electric field is always applied along the z-axis, normal to the plane of the bilayer. Molecular graphics images were generated with Visual Molecular Dynamics (VMD) (Humphrey et al. 1996).

Results and Discussion

Subnanosecond pulse-induced activation of neurons

Fewer than 50, 320 ps, 5 MV/m pulses are sufficient to activate a hippocampal neuron (Fig. 3, -100 pA trace). Although the exploratory experiments reported here were not designed to determine the pulse-number dose response, we can see that when a current-clamped cell is just slightly depolarized with a 20 pA step, the action potential appears even more quickly, after fewer than 10 pulses (Fig. 3, -80 pA trace). Further depolarization causes an immediate action potential (before pulse delivery) followed by a refractory state. In these conditions picosecond pulses result in further depolarization but no action potential (Fig. 3, traces for 0 pA, -20 pA, -40 pA, -60 pA).

Subnanosecond pulse-induced calcium transients in neuroblastoma cells

A single 500 ps, 19 MV/m pulse causes an immediate 10 nM increase (small but detectable) in intracellular Ca^{2+} concentration in NG108 rat neuroblastoma-glioma hybrid cells (Fig. 4). This $[Ca^{2+}]_i$ increase is dose-dependent. A five-pulse exposure (pulse repetition rate = 1 kHz) increases $[Ca^{2+}]_i$ about five times as much as one pulse (fig. 4). For a single pulse, higher pulse amplitudes (up to 30 MV/m) cause larger increases in $[Ca^{2+}]_i$ (data not shown). Cytosolic calcium levels remain elevated for at least 100 s after a single 500 ps pulse.

Subnanosecond electropore formation in molecular simulations of POPC bilayers

In order to see what restructuring of the membrane might occur on a subnanosecond time scale, we carried out MD simulations of POPC bilayers in high electric fields. With applied fields greater than 1.5 GV/m, lipid electropore formation occurs in less than 1 ns (Fig. 5). The pore construction process is similar to that observed with lower fields (Levine and Vernier 2010). In some simulations a pore appears in less than 50 ps. This is not surprising, since it is known that lipid electropore initiation is a stochastic event and that pore initiation time is an exponential function of the electric field (Vernier et al. 2006b; Böckmann et al. 2008).

It should be kept in mind that in an aqueous system the magnitude of the effective electric field is determined in part by the dielectric permittivity of water. At low frequencies the effective field is approximately 1/80 the value of the "applied" (vacuum) field, which means that the field delivered by the pulse generator in an equivalent experimental system will be approximately 1/80 of the value of the external ("vacuum") field specified in a simulation. For 1.5 GV/m in a simulation, for example, the corresponding field in an experiment (electrode voltage divided by electrode separation for a parallel plate configuration) would be approximately 19 MV/m, within the range required for bioelectric effects with "few nanosecond" and picosecond pulses, and similar to the field used in the experiments reported here.

The actual conditions of both our experiments and our simulations, however, are more complicated. First, we are working at frequencies or on time scales where the relative dielectric permittivity of water is much less than 80 (Barthel et al. 1990). Second, the intrusion of individual water molecules from the complex dielectric landscape of the

membrane interface to the low-permittivity environment of the lipid bilayer interior is a phenomenon much better treated in atomic detail, where macroscale material properties like permittivity are of limited utility (Tokman et al. 2013).

Subnanosecond lipid bilayer perturbation with picosecond (terahertz) alternating electric fields

With these same porating electric fields, water intrusion and permeabilization of POPC bilayers occurs within tens of picoseconds even when the polarity of the applied electric field is reversed every picosecond (Fig. 6), a terahertz repetition rate. What we observe under these alternating field conditions, however, rather than the typical formation of a single lipid pore that we see when a non-varying electric field is applied to our very small simulated area (50 nm^2), is a more general disorganization of the bilayer, with numerous individual water bridges instead of one or two, even in this small area, and a more scattered, less determinate distribution of phospholipid head groups across the bilayer interior. Instead of a discrete pore we see a scrambled, disordered mixture of water and phospholipid.

Intuitively we might expect that each picosecond reversal of the electric field direction would "undo" whatever rearrangement had occurred in the preceding cycle, with no net effect. In addition, since the textbook water dipole relaxation time is on the order of 8 ps (Buchner et al. 1999), we might think that water molecule orientation should not be appreciably affected by symmetrical electric field reversals occurring at 1 ps intervals. Finally, interactions of water dipoles with phospholipid head groups retards the reorientation of interfacial water in an applied electric field (Pal, Balasubramanian, Bagchi 2004; Tielrooij et al. 2009). What happens in the simulations is contrary to these expectations. The stabilization of intruding interfacial water by the applied electric field (Tokman et al. 2013) is not reversed when the field direction changes. The water bridges grow, rather than shrink, cycle after cycle, drawing the phospholipid head groups after them.

A closer look reveals how this can be. Note the orientation of the water molecules in the low-permittivity bilayer interior in the two panels of Fig. 7. They rotate to align with the alternating electric field in less than 1 ps. Since there is no hydrogen-bonded network in this local environment to constrain the motion of individual water molecules, the effective relaxation time is much less than it is in bulk water. Water dipole rotation is *retarded* by interactions with interfacial lipids and proteins (Sterpone et al. 2006), but the isolated water molecules that stack up in the membrane interior during pore initiation have escaped their interfacial associations. A field-stabilized water column penetrating the membrane remains a lower energy configuration for interfacial water than the planar lipid-water junction of an unperturbed bilayer regardless of the 180-degree flips of the individual molecules making up the structures.

These simulations provide a plausible mechanism for the permeabilizing restructuring of biological membranes by subnanosecond electric pulses and by rapidly alternating electric fields, even into the terahertz spectral range.

Reconciliation of experimental observations of cellular responses to subnanosecond pulse exposures with molecular simulations of phospholipid bilayers in strong, rapidly changing electric fields

Although other interpretations are possible, the experimental data presented here are consistent with cell membrane permeabilization by subnanosecond electric pulses, with subsequent depolarization of neurons through the discharge of ion concentration gradients and the triggering of an action potential. This subnanosecond electropermeabilization, however, seems different from those seen after exposure to somewhat longer pulses — 600 ns or 60 ns. Specifically, the permeabilizing structures associated with the subnanosecond electroporation reported here (Fig. 3) appear to seal (membrane conductance recovers) much faster (within 20 ms) than those observed after 600 ns (Fig. 1 in (Pakhomov et al. 2009)) or 60 ns (Fig. 2 in (Ibey et al. 2010)) pulse exposure, where membrane conductance remained low for 60 s or more.

Membrane depolarization by ion transport through lipid electropores

Simulations and experimental evidence indicate that transmembrane electric fields can cause the formation of membrane pores with diameters on the order of 1–2 nm (Gurtovenko and Vattulainen 2007; Marrink et al. 2009; Nesin et al. 2010; Romeo et al. 2012) and that the time for pore formation, an exponential function of the applied electric field, can be less than a nanosecond (Levine and Vernier 2010). Molecular simulations of ion transport through lipid electropores have shown that the electrical conductance of these pores is comparable to the conductance of lipid pores determined experimentally (Ho et al. 2013). It seems reasonable to consider whether ion transport through nanoscale lipid electropores formed by nanosecond or subnanosecond electric pulse exposure could be sufficient to depolarize the cell membrane.

For a spherical cell with radius 10 μm, assuming a membrane capacitance of 1×10^{-2} F·m^{-2}, an imbalance of 8×10^6 integral charges (monovalent ions) will create a transmembrane potential of 100 mV. This potential can be discharged (depolarizing the cell membrane) by transporting 8×10^6 positive or negative ions into or out of the cell, as appropriate, depending on the polarities chosen. Normally the potential inside the cell is negative with reference to the extracellular medium, so we could discharge -100 mV, for example, by transporting 8×10^6 Na$^+$ from the medium into the cell.

Neglecting the relatively small electrophoretic transport of ions through pores while the field is applied (because the pulse duration is so short), and considering only diffusive transport through pores remaining after the pulse, we can estimate the rate of diffusion through a lipid electropore by assuming a simple pore geometry and using the approximate method of Hille (Hille 2001). For [Na$^+$] = 150 mM, r_{pore} = 1 nm, D_{Na+} = 1.33×10^{-9} m^2·s^{-1}, l_{pore} = 5 nm, we obtain a diffusion transport rate of 5.7×10^7 Na$^+$ s^{-1} for a single pore. At that rate a single lipid electropore will transport enough Na$^+$ to depolarize the membrane in less than 150 ms. (Numbers for K$^+$ and Cl$^-$ are in the same range.) If we conclude from the membrane voltage traces in Fig. 3 that the pore lifetime is shorter than 150 ms, say on the order of 10 ms, as a rough approximation, we still need only 15 pores to depolarize the membrane. For the very short pore lifetimes around 100 ns seen in simulations of simple phospholipid

bilayers (not cell membranes) (Levine and Vernier 2012), about 1.4×10^6 pores would be required to discharge the membrane. Although we have at this time no solid method for determining electropore densities or total numbers experimentally, continuum pore models of electroporation predict that nanosecond pulses do indeed produce millions of nanometer-scale pores in cells of similar size (Son et al. 2014). These estimates are of course tentative and speculative, but they are specific enough to stimulate further efforts to improve both the models and the experimental efforts.

Calcium transients after subnanosecond pulse exposure

Subnanosecond pulse-induced increases in intracellular calcium concentration could come from influx of extracellular calcium through either the picosecond pulse-permeabilized membrane or voltage-activated calcium channels triggered by the permeabilization-driven depolarization, similar to what has been reported previously for adrenal chromaffin cells (Craviso et al. 2012), and possibly also through calcium-induced calcium release from intracellular stores (Semenov et al. 2013). It cannot be excluded that some or all of the calcium influx comes through calcium channels directly activated by the picosecond pulsed electric field, but it seems unlikely that a protein channel could be activated on this time scale.

Picosecond permeabilizing electric fields

The molecular simulation results presented here provide a plausible physical mechanism for membrane permeabilization by subnanosecond stimuli — water intrusion and bridge formation, accompanied by phospholipid redistribution into the water defect regions. The apparent discrepancy between the somewhat larger fields employed in the MD simulations and the smaller fields used experimentally may be addressed in the following way. For a given transmembrane potential (or the corresponding applied electric field) there is a certain probability of lipid pore formation over a given area over a given time interval. This probability of pore formation increases *exponentially* with transmembrane voltage (applied field) (Vernier et al. 2013). Computational constraints on simulations of hydrated lipid bilayer systems with atomic resolution permit us to sample only a very small area compared to experimental observations. The membrane area for the simulations reported here (about 50 nm^2) represents a fraction of only 10^{-7} of the area of a typical cell membrane. This very small observational window means that to "see" an event that would produce thousands of pores in a cell, we must increase the probability of the event by a factor of several thousand (or run thousands of simulations), and we effectively accomplish that by increasing the applied field.

Thermal effects

The possibility that the responses of cells (and membranes) to repetitive, high-field electric pulses are a consequence of temperature increases in the system must always be considered, especially when large numbers of pulses at high repetition rates are required to produce a given effect. Because the pulses are so few and so short, the total electric pulse energy in the experiments reported here, even if it were completely converted to heat, would increase the temperature of the exposed regions only by about 0.5 K with worst case assumptions.

Simulation temperatures are regulated by a thermostat. Thus any temperature changes that may be occurring in the experiments or in the simulations are small and brief. However, we are adding energy, which results in a change in the properties of the cell membranes and lipid bilayers and a physical redistribution of their components. It may be instructive to think of this membrane electropermeabilization as a phase change, or a physical change of state, that is isothermal but which involves an increase in the energy of the system.

Summary

Subnanosecond (500 ps) electric pulses activate rat hippocampal neurons and trigger calcium transients in NG108 rat neuroblastoma-glioma hybrid cells. Molecular simulations of phospholipid bilayers in electric fields show lipid electropore formation and membrane disorganization in less than 1 ns. Water dipoles in the membrane interior orient in permeabilizing electric fields on a picosecond time scale, consistent with a mechanism involving energy-minimizing intrusions of interfacial water leading to membrane permeabilization by picosecond electric pulses and terahertz electromagnetic fields.

Acknowledgments

References

Abidor IG, Arakelyan VB, Chernomordik LV, Chizmadzhev YA, Pastushenko VF, Tarasevich MR. Electric breakdown of bilayer lipid membranes I. Main experimental facts and their qualitative discussion. Bioelectrochemistry and Bioenergetics. 1979; 6:37–52.

Albini M, Dinarelli S, Pennella F, Romeo S, Zampetti E, Girasole M, Morbiducci U, Massa R, Ramundo-Orlando A. Induced movements of giant vesicles by millimeter wave radiation. Biochim Biophys Acta. 2014; 1838:1710–8. [PubMed: 24704354]

Barthel J, Bachhuber K, Buchner R, Hetzenauer H. Dielectric spectra of some common solvents in the microwave region. Water and lower alcohols. Chemical Physics Letters. 1990; 165:369–373.

Batista Napotnik T, Wu YH, Gundersen MA, Miklavcic D, Vernier PT. Nanosecond electric pulses cause mitochondrial membrane permeabilization in Jurkat cells. Bioelectromagnetics. 2012; 33:257–64. [PubMed: 21953203]

Benz R, Zimmermann U. Pulse-length dependence of the electrical breakdown in lipid bilayer membranes. Biochim Biophys Acta. 1980; 597:637–42. [PubMed: 7378404]

Bockmann RA, de Groot BL, Kakorin S, Neumann E, Grubmuller H. Kinetics, statistics, and energetics of lipid membrane electroporation studied by molecular dynamics simulations. Biophys J. 2008; 95:1837–50. [PubMed: 18469089]

Buchner R, Barthel J, Stauber J. The dielectric relaxation of water between 0 degrees C and 35 degrees C. Chemical Physics Letters. 1999; 306:57–63.

Camp JT, Jing Y, Zhuang J, Kolb JF, Beebe SJ, Song JH, Joshi RP, Xiao S, Schoenbach KH. Cell death induced by subnanosecond pulsed electric fields at elevated temperatures. IEEE Transactions on Plasma Science. 2012; 40:2334–2347.

Chizmadzhev YA, Abidor IG. Bilayer lipid membranes in strong electric fields. Bioelectrochemistry and Bioenergetics. 1980; 7:83–100.

Coster HGL. A quantitative analysis of the voltage-current relationships of fixed charge membranes and the associated property of "punch-through". Biophys J. 1965; 5:669–86. [PubMed: 5863437]

Craviso GL, Choe S, Chatterjee I, Vernier PT. Modulation of intracellular Ca^{2+} levels in chromaffin cells by nanoelectropulses. Bioelectrochemistry. 2012; 87:244–52. [PubMed: 22197468]

Craviso GL, Choe S, Chatterjee P, Chatterjee I, Vernier PT. Nanosecond electric pulses: a novel stimulus for triggering Ca^{2+} influx into chromaffin cells via voltage-gated Ca^{2+} channels. Cell Mol Neurobiol. 2010; 30:1259–65. [PubMed: 21080060]

Frandsen SK, Gissel H, Hojman P, Tramm T, Eriksen J, Gehl J. Direct therapeutic applications of calcium electroporation to effectively induce tumor necrosis. Cancer Res. 2012; 72:1336–41. [PubMed: 22282658]

Gowrishankar TR, Weaver JC. An approach to electrical modeling of single and multiple cells. Proc Natl Acad Sci U S A. 2003; 100:3203–8. [PubMed: 12626744]

Gurtovenko AA, Vattulainen I. Pore formation coupled to ion transport through lipid membranes as induced by transmembrane ionic charge imbalance: atomistic molecular dynamics study. J Am Chem Soc. 2005; 127:17570–1. [PubMed: 16351063]

Gurtovenko AA, Vattulainen I. Ion leakage through transient water pores in protein-free lipid membranes driven by transmembrane ionic charge imbalance. Biophys J. 2007; 92:1878–90. [PubMed: 17208976]

Heller LC, Heller R. In vivo electroporation for gene therapy. Hum Gene Ther. 2006; 17:890–7. [PubMed: 16972757]

Hess B, Kutzner C, van der Spoel D, Lindahl E. GROMACS 4: Algorithms for highly efficient, load-balanced, and scalable molecular simulation. Journal of Chemical Theory and Computation. 2008; 4:435–447.

Hille, B. Ion channels of excitable membranes. Sinauer Associates; 2001.

Hintzsche H, Jastrow C, Heinen B, Baaske K, Kleine-Ostmann T, Schwerdtfeger M, Shakfa MK, Karst U, Koch M, Schrader T, Stopper H. Terahertz radiation at 0.380 THz and 2.520 THz does not lead to DNA damage in skin cells in vitro. Radiat Res. 2013; 179:38–45. [PubMed: 23181591]

Ho MC, Casciola M, Levine ZA, Vernier PT. Molecular dynamics simulations of ion conductance in field-stabilized nanoscale lipid electropores. J Phys Chem B. 2013; 117:11633–40. [PubMed: 24001115]

Humphrey W, Dalke A, Schulten K. VMD: visual molecular dynamics. J Mol Graph. 1996; 14:33–8. 27–8. [PubMed: 8744570]

Ibey BL, Mixon DG, Payne JA, Bowman A, Sickendick K, Wilmink GJ, Roach WP, Pakhomov AG. Plasma membrane permeabilization by trains of ultrashort electric pulses. Bioelectrochemistry. 2010; 79:114–21. [PubMed: 20171148]

Ibey BL, Roth CC, Pakhomov AG, Bernhard JA, Wilmink GJ, Pakhomova ON. Dose-dependent thresholds of 10-ns electric pulse induced plasma membrane disruption and cytotoxicity in multiple cell lines. PLoS One. 2011; 6:e15642. [PubMed: 21390200]

Kim KT, Park J, Jo SJ, Jung S, Kwon OS, Gallerano GP, Park WY, Park GS. High-power femtosecond-terahertz pulse induces a wound response in mouse skin. Sci Rep. 2013; 3:2296. [PubMed: 23907528]

Koronkiewicz S, Kalinowski S, Bryl K. Programmable chronopotentiometry as a tool for the study of electroporation and resealing of pores in bilayer lipid membranes. Biochim Biophys Acta. 2002; 1561:222–9. [PubMed: 11997122]

Kotnik T, Miklavcic D. Second-order model of membrane electric field induced by alternating external electric fields. IEEE Trans Biomed Eng. 2000; 47:1074–81. [PubMed: 10943056]

Levine ZA, Vernier PT. Life cycle of an electropore: field-dependent and field-independent steps in pore creation and annihilation. J Membr Biol. 2010; 236:27–36. [PubMed: 20623350]

Levine ZA, Vernier PT. Calcium and phosphatidylserine inhibit lipid electropore formation and reduce pore lifetime. J Membr Biol. 2012; 245:599–610. [PubMed: 22815071]

Marrink SJ, de Vries AH, Tieleman DP. Lipids on the move: Simulations of membrane pores, domains, stalks and curves. Biochim Biophys Acta. 2009; 1788:149–68. [PubMed: 19013128]

Marty M, Sersa G, Garbay JR, Gehl J, Collins CG, Snoj M, Billard V, Geertsen PF, Larkin JO, Miklavcic D, Pavlovic I, Paulin-Kosir SM, Cemazar M, Morsli N, Rudolf Z, Robert C, O'Sullivan

GC, Mir LM. Electrochemotherapy - An easy, highly effective and safe treatment of cutaneous and subcutaneous metastases: Results of ESOPE (European Standard Operating Procedures of Electrochemotherapy) study. European Journal of Cancer Supplements. 2006; 4:3–13.

Melikov KC, Frolov VA, Shcherbakov A, Samsonov AV, Chizmadzhev YA, Chernomordik LV. Voltage-induced nonconductive pre-pores and metastable single pores in unmodified planar lipid bilayer. Biophys J. 2001; 80:1829–36. [PubMed: 11259296]

Napotnik TB, Rebersek M, Kotnik T, Lebrasseur E, Cabodevila G, Miklavcic D. Electropermeabilization of endocytotic vesicles in B16 F1 mouse melanoma cells. Med Biol Eng Comput. 2010; 48:407–13. [PubMed: 20361267]

Naumowicz M, Figaszewski ZA. Pore formation in lipid bilayer membranes made of phosphatidylcholine and cholesterol followed by means of constant current. Cell Biochem Biophys. 2013; 66:109–19. [PubMed: 23104105]

Nesin OM, Pakhomova ON, Xiao S, Pakhomov AG. Manipulation of cell volume and membrane pore comparison following single cell permeabilization with 60- and 600-ns electric pulses. Biochim Biophys Acta. 2010; 1808:792–801. [PubMed: 21182825]

Neu JC, Krassowska W. Asymptotic model of electroporation. Physical Review E. 1999; 59:3471–3482.

Neumann E, Schaefer-Ridder M, Wang Y, Hofschneider PH. Gene transfer into mouse lyoma cells by electroporation in high electric fields. EMBO J. 1982; 1:841–5. [PubMed: 6329708]

Nuccitelli R, Pliquett U, Chen X, Ford W, Swanson RJ, Beebe SJ, Kolb JF, Schoenbach KH. Nanosecond pulsed electric fields cause melanomas to self-destruct. Biochem Biophys Res Commun. 2006; 343:351–60. [PubMed: 16545779]

Pakhomov AG, Bowman AM, Ibey BL, Andre FM, Pakhomova ON, Schoenbach KH. Lipid nanopores can form a stable, ion channel-like conduction pathway in cell membrane. Biochem Biophys Res Commun. 2009; 385:181–6. [PubMed: 19450553]

Pakhomov AG, Kolb JF, White JA, Joshi RP, Xiao S, Schoenbach KH. Long-lasting plasma membrane permeabilization in mammalian cells by nanosecond pulsed electric field (nsPEF). Bioelectromagnetics. 2007a; 28:655–63. [PubMed: 17654532]

Pakhomov AG, Shevin R, White JA, Kolb JF, Pakhomova ON, Joshi RP, Schoenbach KH. Membrane permeabilization and cell damage by ultrashort electric field shocks. Arch Biochem Biophys. 2007b; 465:109–18. [PubMed: 17555703]

Pakhomova ON, Khorokhorina VA, Bowman AM, Rodaite-Riseviciene R, Saulis G, Xiao S, Pakhomov AG. Oxidative effects of nanosecond pulsed electric field exposure in cells and cell-free media. Arch Biochem Biophys. 2012; 527:55–64. [PubMed: 22910297]

Pal S, Balasubramanian S, Bagchi B. Anomalous dielectric relaxation of water molecules at the surface of an aqueous micelle. J Chem Phys. 2004; 120:1912–20. [PubMed: 15268325]

Ramundo-Orlando A, Gallerano GP. Terahertz radiation effects and biological applications. Journal of Infrared Millimeter and Terahertz Waves. 2009; 30:1308–1318.

Ramundo-Orlando A, Gallerano GP, Stano P, Doria A, Giovenale E, Messina G, Cappelli M, D'Arienzo M, Spassovsky I. Permeability changes induced by 130 GHz pulsed radiation on cationic liposomes loaded with carbonic anhydrase. Bioelectromagnetics. 2007; 28:587–98. [PubMed: 17620303]

Rols MP. Electropermeabilization, a physical method for the delivery of therapeutic molecules into cells. Biochim Biophys Acta. 2006; 1758:423–428. [PubMed: 16483538]

Romanenko S, Siegel PH, Wagenaar DA, Pikov V. Effects of millimeter wave irradiation and equivalent thermal heating on the activity of individual neurons in the leech ganglion. J Neurophysiol. 2014; 112:2423–31. [PubMed: 25122711]

Romeo S, Wu YH, Levine ZA, Gundersen MA, Vernier PT. Water influx and cell swelling after nanosecond electropermeabilization. Biochim Biophys Acta. 2013; 1828:1715–1722. [PubMed: 23500618]

Schoenbach KH, Beebe SJ, Buescher ES. Intracellular effect of ultrashort electrical pulses. Bioelectromagnetics. 2001; 22:440–8. [PubMed: 11536285]

Schoenbach KH, Xiao S, Joshi RP, Camp JT, Heeren T, Kolb JF, Beebe SJ. The effect of intense subnanosecond electrical pulses on biological cells. IEEE Transactions on Plasma Science. 2008; 36:414–422.

Semenov I, Xiao S, Pakhomov AG. Primary pathways of intracellular Ca^{2+} mobilization by nanosecond pulsed electric field. Biochim Biophys Acta. 2013; 1828:981–9. [PubMed: 23220180]

Silve A, Leray I, Mir LM. Demonstration of cell membrane permeabilization to medium-sized molecules caused by a single 10 ns electric pulse. Bioelectrochemistry. 2012; 87:260–4. [PubMed: 22074790]

Son RS, Smith KC, Gowrishankar TR, Vernier PT, Weaver JC. Basic features of a cell electroporation model: illustrative behavior for two very different pulses. J Membr Biol. 2014; 247:1209–28. [PubMed: 25048527]

Sterpone F, Marchetti G, Pierleoni C, Marchi M. Molecular modeling and simulation of water near model micelles: diffusion, rotational relaxation and structure at the hydration interface. J Phys Chem B. 2006; 110:11504–10. [PubMed: 16771426]

Sugar IP, Neumann E. Stochastic model for electric field-induced membrane pores. Electroporation. Biophys Chem. 1984; 19:211–25. [PubMed: 6722274]

Tarek M. Membrane electroporation: a molecular dynamics simulation. Biophys J. 2005; 88:4045–4053. [PubMed: 15764667]

Teissie J, Golzio M, Rols MP. Mechanisms of cell membrane electropermeabilization: a minireview of our present (lack of ?) knowledge. Biochim Biophys Acta. 2005; 1724:270–80. [PubMed: 15951114]

Teissie J, Rols MP. An experimental evaluation of the critical potential difference inducing cell membrane electropermeabilization. Biophys J. 1993; 65:409–13. [PubMed: 8369446]

Tekle E, Oubrahim H, Dzekunov SM, Kolb JF, Schoenbach KH, Chock PB. Selective field effects on intracellular vacuoles and vesicle membranes with nanosecond electric pulses. Biophys J. 2005; 89:274–84. [PubMed: 15821165]

Tieleman DP. The molecular basis of electroporation. BMC Biochem. 2004; 5:10. [PubMed: 15260890]

Tielrooij KJ, Paparo D, Piatkowski L, Bakker HJ, Bonn M. Dielectric relaxation dynamics of water in model membranes probed by terahertz spectroscopy. Biophys J. 2009; 97:2484–92. [PubMed: 19883591]

Timoshkin IV, MacGregor SJ, Fouracre RA, Crichton BH, Anderson JG. Transient electrical field across cellular membranes: pulsed electric field treatment of microbial cells. Journal of Physics D-Applied Physics. 2006; 39:596–603.

Titova LV, Ayesheshim AK, Golubov A, Fogen D, Rodriguez-Juarez R, Hegmann FA, Kovalchuk O. Intense THz pulses cause H2AX phosphorylation and activate DNA damage response in human skin tissue. Biomed Opt Express. 2013a; 4:559–68. [PubMed: 23577291]

Titova LV, Ayesheshim AK, Golubov A, Rodriguez-Juarez R, Woycicki R, Hegmann FA, Kovalchuk O. Intense THz pulses down-regulate genes associated with skin cancer and psoriasis: a new therapeutic avenue? Sci Rep. 2013b; 3:2363. [PubMed: 23917523]

Tokman M, Lee JH, Levine ZA, Ho MC, Colvin ME, Vernier PT. Electric field-driven water dipoles: nanoscale architecture of electroporation. PLoS One. 2013; 8:e61111. [PubMed: 23593404]

Tolstykh GP, Beier HT, Roth CC, Thompson GL, Ibey BL. 600 ns pulse electric field-induced phosphatidylinositol$_{4,5}$-bisphosphate depletion. Bioelectrochemistry. 2014; 100:80–7. [PubMed: 24530104]

Vernier PT, Levine ZA, Gundersen MA. Water bridges in electropermeabilized phospholipid bilayers. Proceedings of the IEEE. 2013; 101:494–504.

Vernier PT, Sun Y, Gundersen MA. Nanoelectropulse-driven membrane perturbation and small molecule permeabilization. BMC Cell Biology. 2006a; 7:37. [PubMed: 17052354]

Vernier PT, Sun Y, Marcu L, Craft CM, Gundersen MA. Nanosecond pulsed electric fields perturb membrane phospholipids in T lymphoblasts. FEBS Lett. 2004; 572:103–8. [PubMed: 15304332]

Vernier PT, Sun Y, Marcu L, Salemi S, Craft CM, Gundersen MA. Calcium bursts induced by nanosecond electric pulses. Biochemical and Biophysical Research Communications. 2003; 310:286–95. [PubMed: 14521908]

Vernier PT, Ziegler MJ, Sun Y, Gundersen MA, Tieleman DP. Nanopore-facilitated, voltage-driven phosphatidylserine translocation in lipid bilayers - in cells and in silico. Physical Biology. 2006b; 3:233–247. [PubMed: 17200599]

Weaver JC, Chizmadzhev YA. Theory of electroporation: a review. Bioelectrochemistry and Bioenergetics. 1996; 41:135–160.

Williams R, Schofield A, Holder G, Downes J, Edgar D, Harrison P, Siggel-King M, Surman M, Dunning D, Hill S, Holder D, Jackson F, Jones J, McKenzie J, Saveliev Y, Thomsen N, Williams P, Weightman P. The influence of high intensity terahertz radiation on mammalian cell adhesion, proliferation and differentiation. Phys Med Biol. 2013; 58:373–91. [PubMed: 23257566]

Wilmink GJ, Rivest BD, Roth CC, Ibey BL, Payne JA, Cundin LX, Grundt JE, Peralta X, Mixon DG, Roach WP. In vitro investigation of the biological effects associated with human dermal fibroblasts exposed to 2.52 THz radiation. Lasers in Surgery and Medicine. 2011; 43:152–163. [PubMed: 20740621]

Xiao S, Guo S, Nesin V, Heller R, Schoenbach KH. Subnanosecond electric pulses cause membrane permeabilization and cell death. IEEE Trans Biomed Eng. 2011; 58:1239–45. [PubMed: 21303739]

Zeni O, Gallerano GP, Perrotta A, Romano M, Sannino A, Sarti M, D'Arienzo M, Doria A, Giovenale E, Lai A, Messina G, Scarfi MR. Cytogenetic observations in human peripheral blood leukocytes following in vitro exposure to THz radiation: a pilot study. Health Phys. 2007; 92:349–57. [PubMed: 17351499]

Zimmermann U, Pilwat G, Riemann F. Dielectric breakdown of cell membranes. Biophys J. 1974; 14:881–99. [PubMed: 4611517]
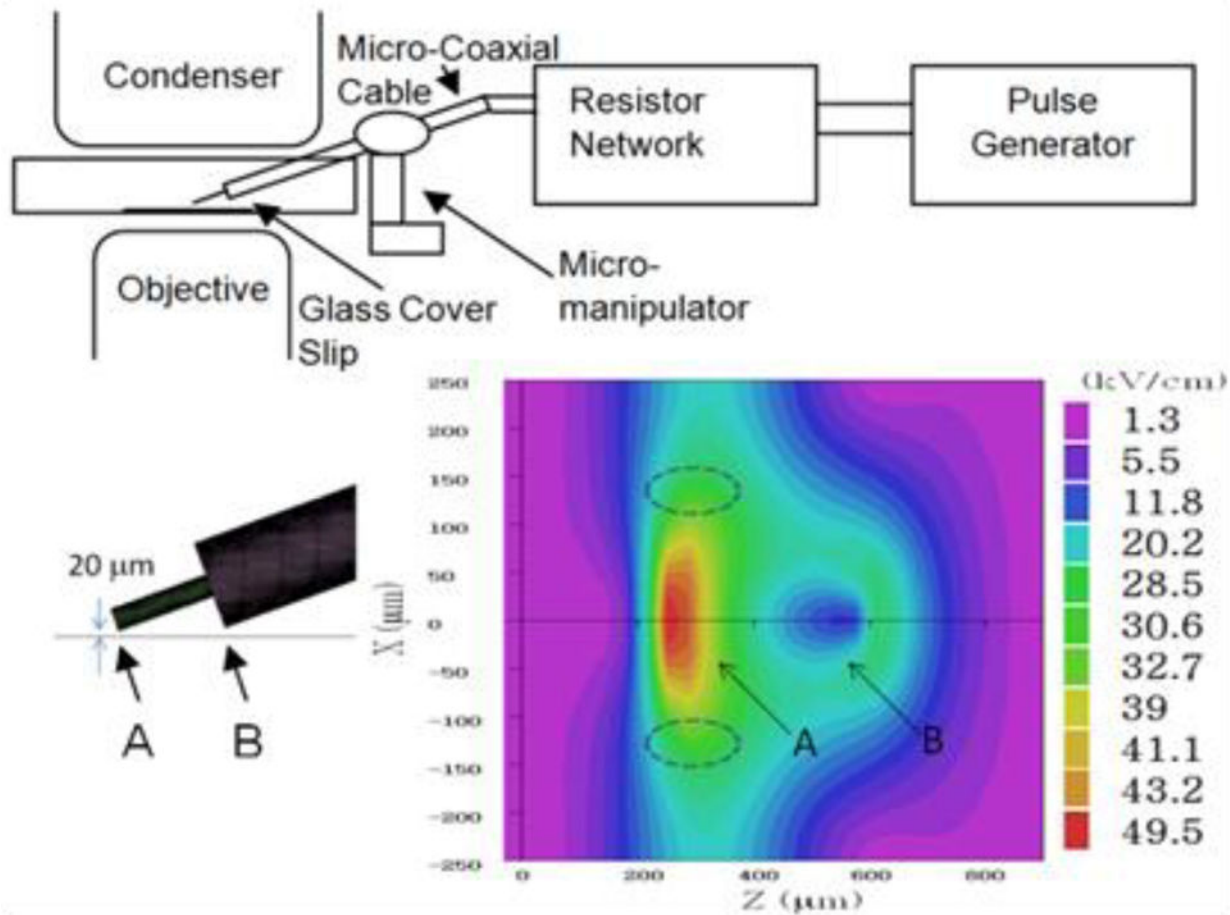
Fig. 1.
Micro-coaxial cable pulse delivery system for neurons on microscope stage. The tip of the
micro-coaxial cable (the inner conductor) is 20 μm above the cover slip. Regions A and B
are projections of the micro-coaxial cable. Cells to be analyzed are within the two off-axis
dashed ellipses. The color map shows the electric field distribution at the surface of the
coverslip for a 1 kV pulse voltage, in which case the electric field in the elliptical areas is
about 3 MV/m.
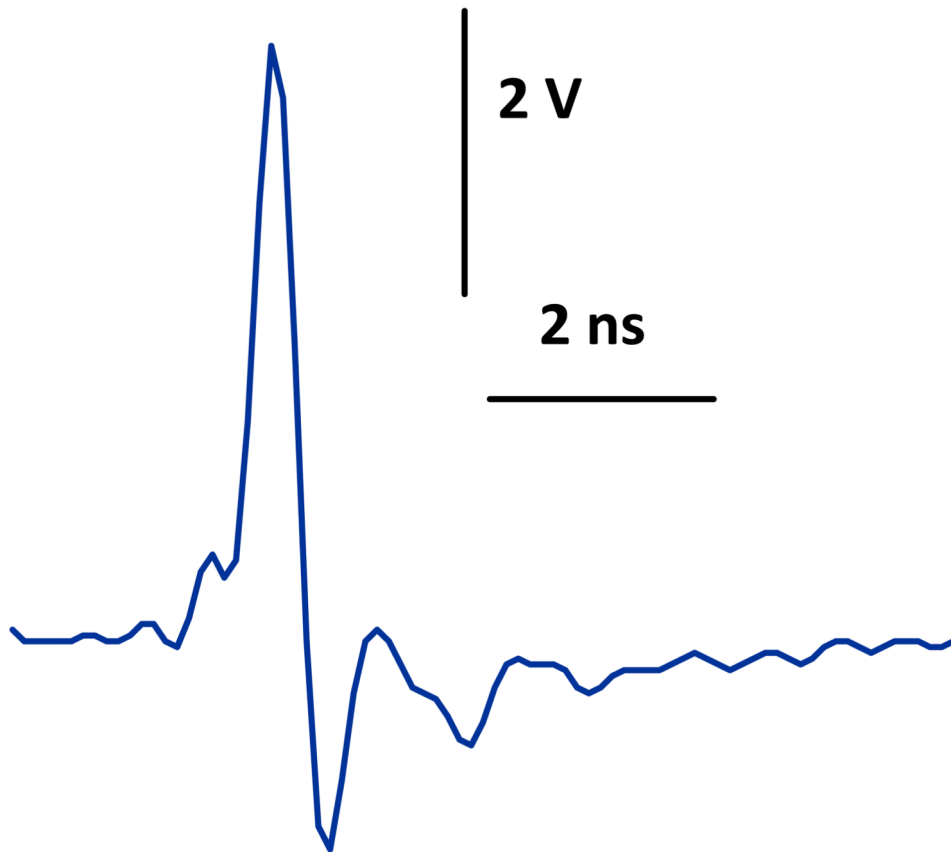
Fig. 2.
Picosecond pulse waveform at the output of the pulse generator. 320 ps (full-width, half-maximum), 5.5 kV.
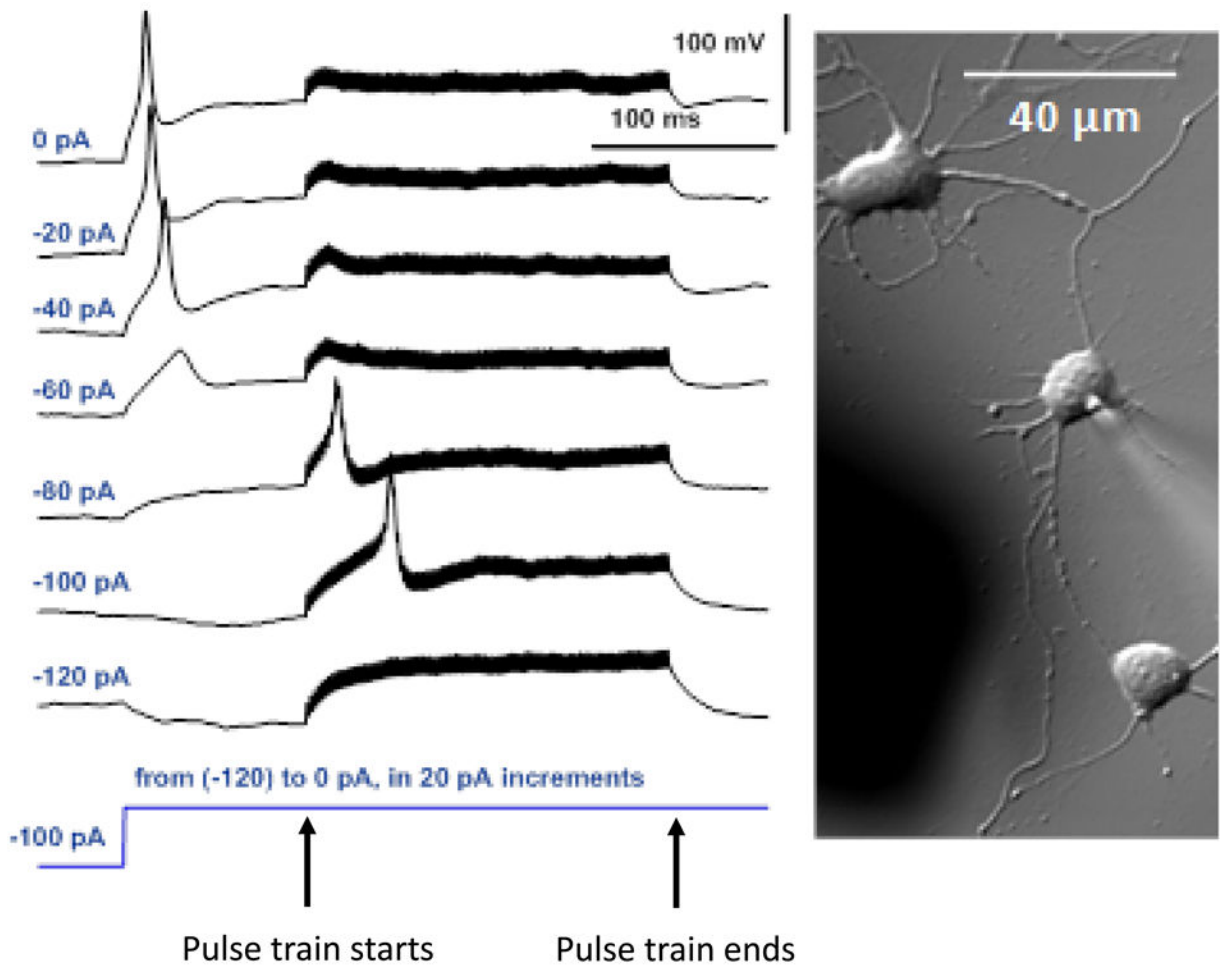
Fig. 3.
Action potentials in a rat hippocampal neuron stimulated by 320 ps electric pulses. Membrane voltage in whole-cell configuration measured in current clamp mode with current stepped in 20 pA increments from the holding level of -100 pA, vertically separated for clarity. Current protocol shown below voltage traces. 100 ms after each current step (arrow), 100 pulses, 5 MV/m, 500 Hz) were delivered over a period of 200 ms. Pulse-induced depolarization and action potentials occurred at the -100 and -80 pA steps. Further depolarization by reducing the injected current immediately caused an action potential followed by a refractory state, so the picosecond pulses produced some additional depolarization without eliciting an action potential. The inset shows the neuron with a recording pipette attached in the vicinity of the pulse-delivering electrode (shadow).
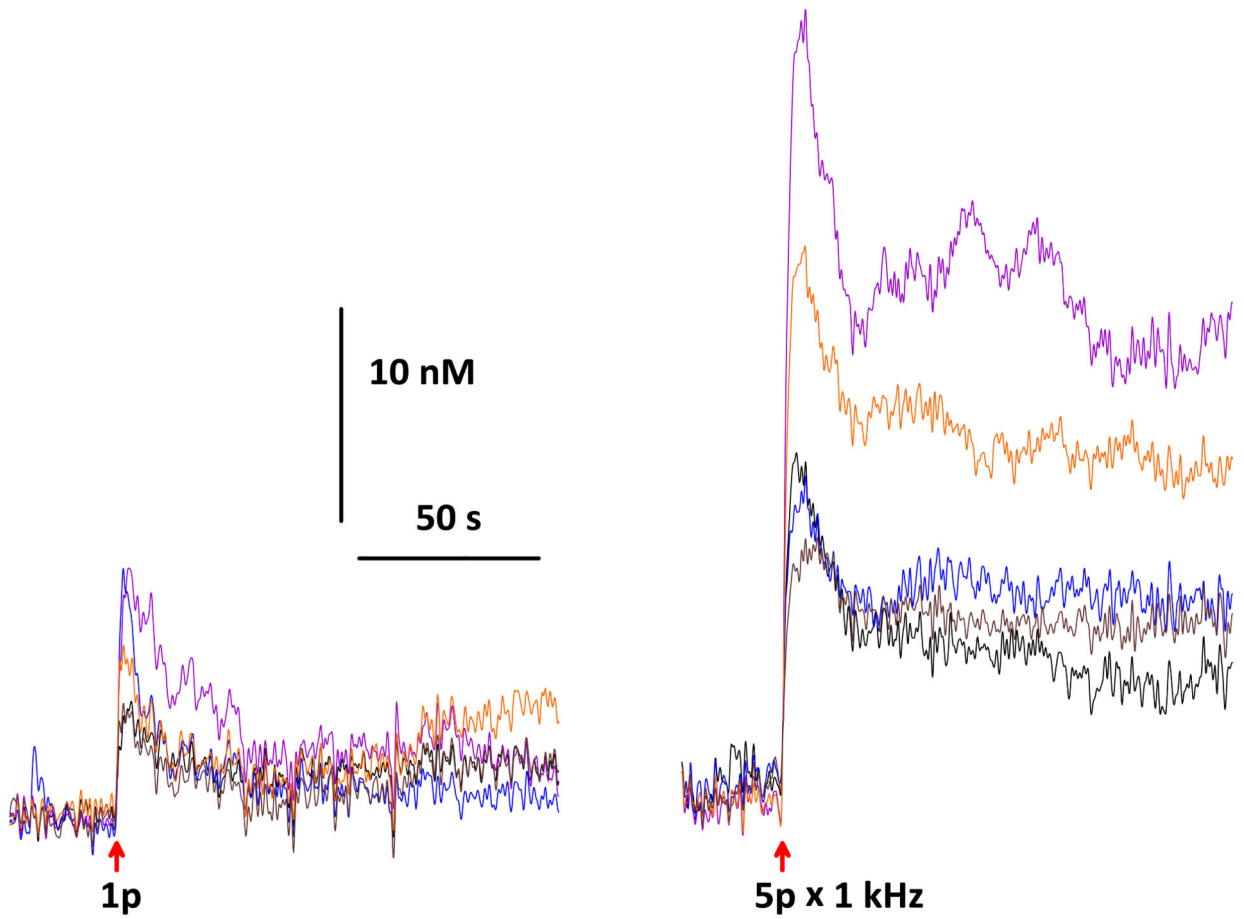
Fig. 4.
Ca^{2+} transients in NG108 rat neuroblastoma-glioma hybrid cells evoked by a single 500 ps, 19 MV/m pulse and a train of 5 pulses at 1 kHz. Measured with Fura-2 ratiometric imaging. Traces from 5 cells superimposed in each panel.
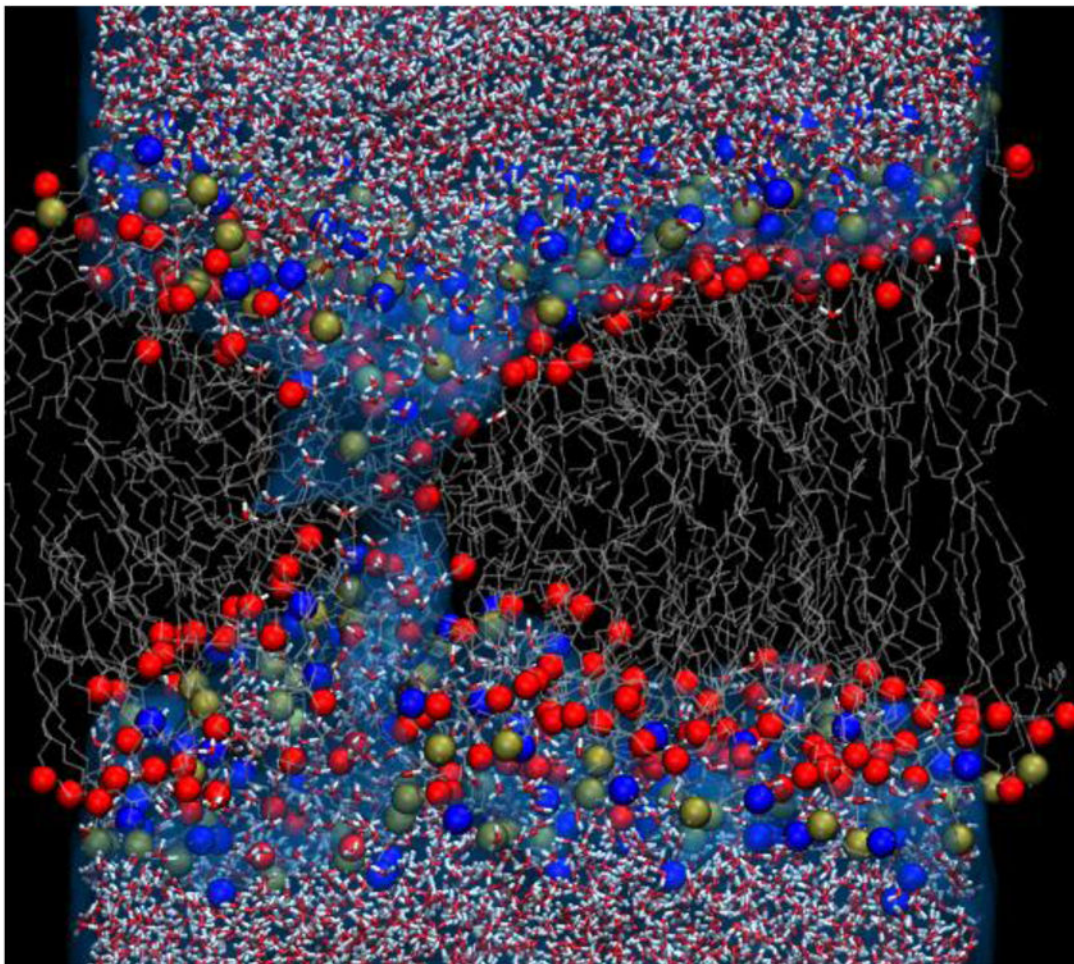
Fig. 5.
Lipid electropore in POPC bilayer forms in less than 1 ns. In this high applied electric field (E_{vacuum} = 2.5 GV/m; $E_{effective}$ = 12.5 MV/m), pore initiation is rapid and a hydrophilic pore is constructed in less than 1 ns. Water molecules (small red and white structures) penetrate the membrane interface and bridge the membrane interior, followed by the phospholipid head groups (blue – nitrogen; gold – phosphorus; red – backbone acyl oxygen). Gray strands are the lipid hydrocarbon tails.

6 ps   12 ps   25 ps   50 ps
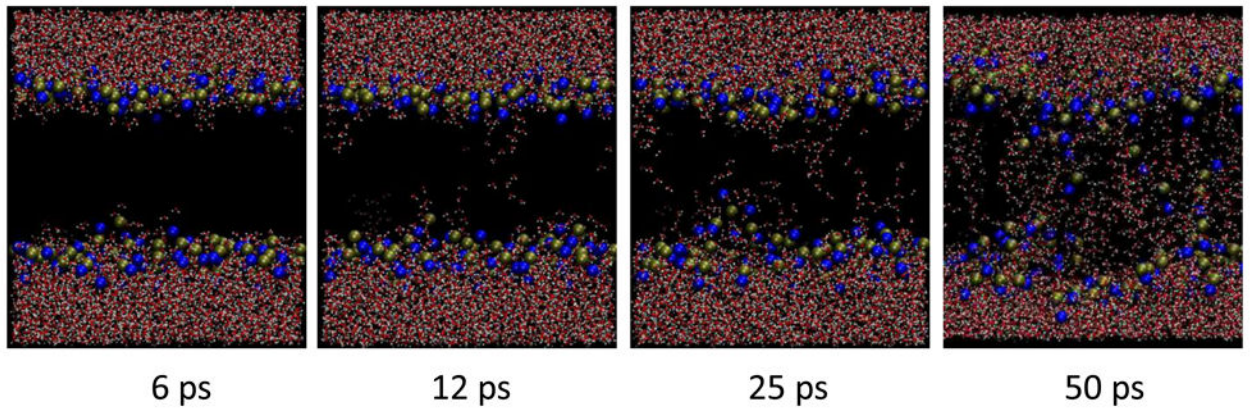
Fig. 6.
Permeabilization of POPC bilayer in 500 GHz alternating electric field. Water, then phospholipid head groups bridge the membrane interior in a very high porating electric field with polarity reversals every picosecond. Multiple water bridges appear, followed by head groups, in a few tens of picoseconds.
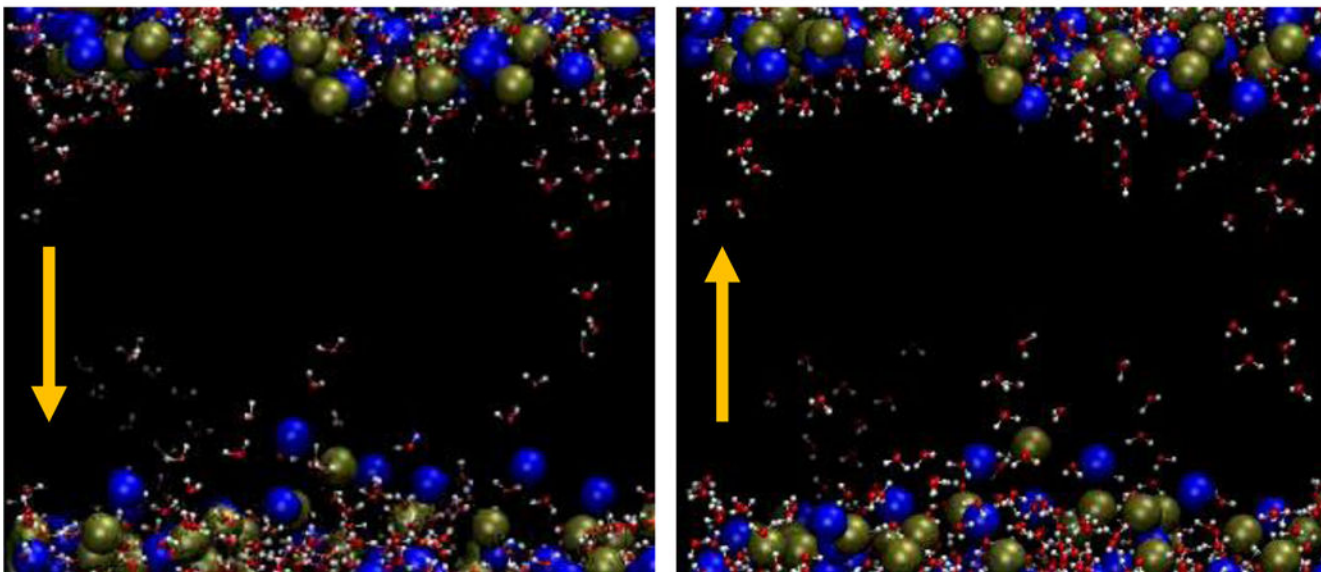
Fig. 7.
Dipole reversal for water molecules in the phospholipid bilayer interior. Note that the oxygen (red) end of each of the bridging water molecules in the middle of the membrane is positioned toward the bottom of the left image and toward the top of the right image. The electric field direction is opposite in these two frames, which are 1 ps apart. Within that 1 ps the water dipoles in the membrane interior align in the new field direction. Dipole relaxation time for water in the membrane interior is much less than in bulk water, so that field-stabilized intruding water columns remain the lower energy configuration for interfacial water.